Lattice strain from substitutional Ga and from holes in heavily doped Si:Ga

K. L. Kavanagh
Department of Electrical and Computer Engineering, University of California at San Diego, La Jolla, California 92093

G. S. Cargill III
IBM Research Division, Thomas J. Watson Research Center, Yorktown Heights, New York 10598

(Received 18 March 1991; revised manuscript received 5 September 1991)

The average lattice strain per Ga atom with respect to pure silicon, $\beta_{\text{total}}=\Delta a/aN_{\text{Ga}}=+(0.9\pm0.1)\times10^{-24}$ cm^3, for heavily doped Si:Ga was measured by high-resolution x-ray diffraction. This strain includes effects of both substitutional Ga atoms in the lattice and doping-related holes in the valence band. The local "size-effect" lattice strain around substitutional Ga atoms, which is not expected to be affected significantly by valence-band holes, was determined from the Ga-to-Si nearest-neighbor distance measured using extended x-ray-absorption fine structure (EXAFS). This distance, $r^{\text{NN}}=2.41\pm0.02$ Å, is 0.06 Å larger than the usual Si-to-Si nearest-neighbor distance and was used to calculate the size-effect contribution per Ga atom to the average lattice strain, $\beta_{\text{size}}=(1.2\pm0.3)\times10^{-24}$ cm^3. This value was subtracted from the overall lattice strain β_{total} to determine the lattice strain per valence-band hole, $\beta_h=-(0.3\pm0.3)\times10^{-24}$ cm^3, and the hydrostatic deformation potential for the valence-band edge in silicon, $a_v=-0.5\pm0.5$ eV. These results were obtained from Si:Ga samples prepared by liquid-phase epitaxy. They were characterized by Rutherford backscattering, ion channeling, electron microscopy, and resistivity measurements, as well as by x-ray diffraction and EXAFS. The samples were of excellent crystal quality, with uniform Ga concentrations of 1.0 and 1.5×10^{20} cm^{-3}, with substitutional fractions greater than 95% and similar electrical resistivities of 2×10^{-3} Ω cm.

I. INTRODUCTION

The effects of substitutional impurities and other defects on lattice strain in semiconductors remain an area of active research. Lattice parameter variations have been studied using x-ray diffraction.[1–6] However, very few direct measurements of the local atomic structure at isolated substitutional impurities have been reported.[6–8]

Using extended x-ray-absorption fine structure (EXAFS) we have measured the Ga-to-Si nearest-neighbor distance in heavily doped Si:Ga. By combining this result with measurements of the overall lattice expansion per Ga atom, we have determined the lattice strain per hole in the valence band and the hydrostatic deformation potential for the valence-band edge. We note that these are measurements for an acceptor impurity in Si.[9] A similar approach was used successfully in studying effects of a donor impurity, As, in Si.[5,6]

Preparation and characterization of heavily doped Si:Ga samples are described in Secs. II A and II B of this paper. These are followed by sections on EXAFS measurements (II C), analysis (II D), and results (II E). The measured Ga-to-Si nearest-neighbor distances are discussed in terms of natural bond lengths and are compared with theoretically predicted bond lengths in Sec. III A. Comparisons among results for Si:Ga, Si:Ge, and Si:As are given in Sec. III B. EXAFS and x-ray rocking curve results for Si:Ga are discussed in terms of lattice strain from holes and in terms of the valence-band deformation potential in Secs. III C and III D, and the conclusions of this paper are summarized in Sec. IV.

II. EXPERIMENTAL PROCEDURE AND RESULTS

A. Sample preparation

Two Si:Ga samples prepared by liquid-phase epitaxy (LPE) are listed in Table I. These were kindly provided by M. Cardona (Max-Planck-Institut, Stuttgart). They were grown on (111) Si wafers at a temperature of 450 °C from Ga-saturated Si melts to thicknesses of 0.6 and 1.8 μm[10]. Measurements with Rutherford backscattering

TABLE I. Data for Si:Ga samples. Tabulated for each sample is total-layer thickness t; substitutional Ga concentration N_{Ga}; sheet resistance R_{sheet}; average resistivity ρ; fractional lattice expansion (333) measured by double-crystal x-ray diffraction, $\Delta d/d$; fractional change in unconstrained lattice constant, $\Delta a/a$; and lattice expansion per Ga atom $\beta_{\text{total}}=\Delta a/aN_{\text{Ga}}$.

t (μm)	N_{Ga} (10^{20} cm^{-3})	R_{sheet} (Ω/□)	ρ (10^{-3} Ω cm)	$\Delta d/d$ (10^{-4})	$\Delta a/a$ (10^{-4})	β_{total} (10^{-24} cm^3)
0.6	0.9±0.1	30±6	1.8±0.4	1.35±0.05	0.94±0.04	0.99±0.1
1.8	1.4±0.1	12±2	2.2±0.4	1.64±0.05	1.15±0.04	0.84±0.1

spectrometry (RBS) and ion channeling for these two samples showed that the Ga was uniformly distributed at concentrations of 1.0 and 1.5×10^{20} cm^{-3} and that the Ga substitutionality was greater than 95%.

B. Characterization of as-prepared samples

Transmission electron microscopy (TEM) was carried out with a Philips EM400 electron microscope operating at 300 keV. In plan view, no precipitates, misfit dislocations, or other extended defects were detected in the Si:Ga material. The absence of misfit dislocations indicates that the Si:Ga layers were coherent with their Si substrates.

Sheet resistances of each sample were measured using an in-line four point probe with appropriate corrections for small sample size. Average resistivities ρ were calculated using the sheet resistances R_{sheet} and the total layer thicknesses t obtained from RBS measurements and x-ray rocking curves. These results, together with substitutional Ga concentrations, are given in Table I. The average values obtained for ρ, $(2.0\pm0.4)\times10^{-3}$ Ω cm, are similar to those reported for Si:Ga prepared by implantation and rapid thermal annealing[11] (RTA) or furnace annealing.[12]

Double-crystal x-ray rocking curves from (333) symmetric reflections were recorded using Cu$K\alpha$ radiation.[1,3–6] A (111)Si reference crystal was used as the first crystal monochromator. Results are shown in Fig. 1. A secondary peak or an asymmetry on the larger substrate peak is observed towards smaller angles, indicating a lattice expansion. The expansion is presumed to be due primarily to Ga, but contributions from intrinsic point defects, particularly self interstitials, cannot be ruled out.

When the substrate and layer diffraction peaks are well separated and the Ga concentration is uniform, the strain can be simply calculated from the peak separation $\Delta\theta$,

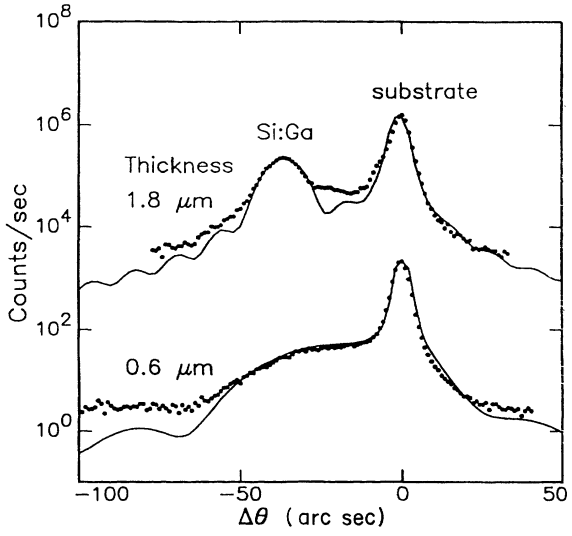

FIG. 1. Double-crystal x-ray rocking curves of Si:Ga samples. The solid lines are simulated spectra. Uniform strain profiles of 1.64 and $1.35\pm0.05\times0.05\times10^{-4}$, 1.8- and 0.6-μm-thick layers, respectively, were used in the simulations.

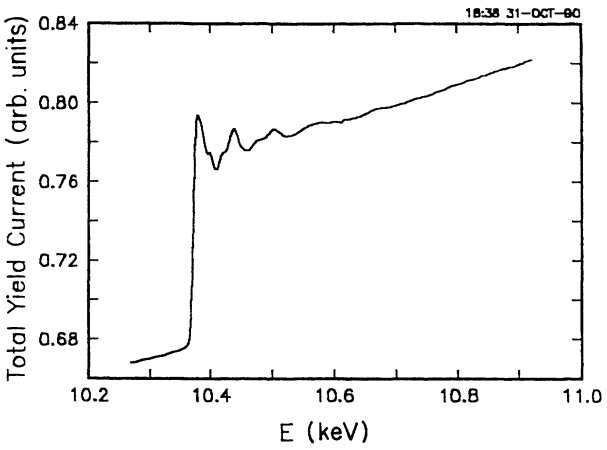

FIG. 2. EXAFS data for a 0.6-μm Si:Ga sample.

$$\frac{\Delta d}{d} = -(\cot\theta)\Delta\theta \ . \tag{1}$$

The Ga-related strain, $\Delta d/d$, in the 1.8-μm-thick LPE sample is thus $(1.64\pm0.05)\times10^{-4}$, in agreement with the result of Ref. 10.

A rocking-curve simulation was also used to determine the strain and film thickness.[1,3,4,6,13] Simulated rocking curves based on a dynamical scattering algorithm[13] have been overlaid with the data (solid lines). Uniform strain profiles with $\Delta d/d$ of $(1.64\pm0.05)\times10^{-4}$ and $(1.35\pm0.05)\times10^{-4}$ provided good fits to the data, as shown in Fig. 1.

The lattice expansions $\Delta d/d$ for each sample are listed in Table I. $\Delta a/a$ can be obtained from $\Delta d/d$ with an appropriate correction for Poisson's expansion 0.70, for (111) substrates.[14] $\Delta a/a$ and the coefficient of lattice expansion, $\beta_{\text{total}}=\Delta a/aN_{\text{Ga}}$, for each sample are also listed in Table I. The results agree to within experimental error with an average value of $\beta_{\text{total}}=(+0.9\pm0.1)\times10^{-24}$ cm^3.

C. EXAFS measurements

EXAFS measurements for the 0.6-μm sample were made at the National Synchrotron Light Source (NSLS)

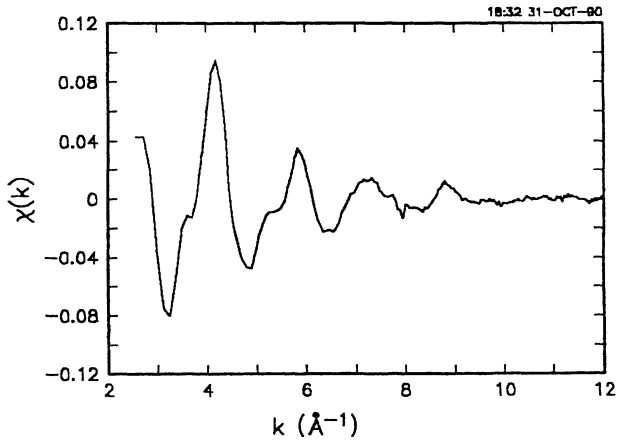

FIG. 3. EXAFS $\chi(k)$ function for 0.6-μm Si:Ga sample.

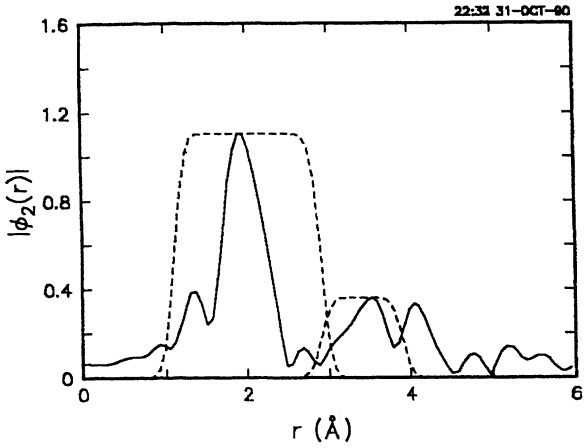

FIG. 4. EXAFS $|\Phi_2(r)|$ function for a Si:Ga sample, including envelope functions used in extracting nearest neighbor $\chi_{NN}(k)$ and next-nearest-neighbor $\chi_{NNN}(k)$ components of $\chi(k)$, which are shown in Figs. 5 and 6.

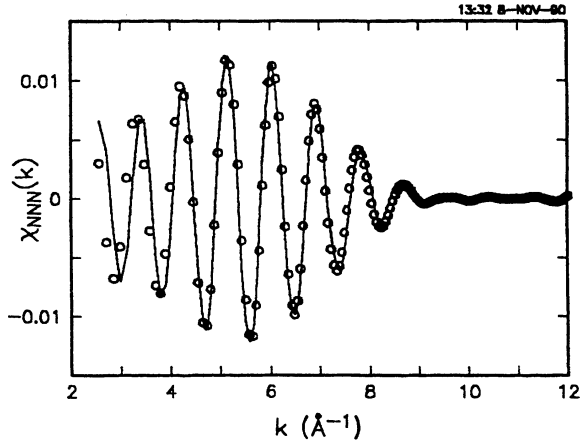

FIG. 6. Next-nearest-neighbor component of $\chi(k)$ for a Si:Ga sample (solid lines). Plotted symbols (○) are fitted model calculations $\chi_{calc}(k)$.

on beamline X23A2 using a Si(220) monochromator. The EXAFS measurements used total-electron-yield detection as described in Ref. 15, except that samples were rocked around two perpendicular axes to eliminate more completely the Bragg diffraction effects. These measurements were used to obtain distances from Ga atoms to their nearest neighbors and next-nearest neighbors.

EXAFS data are shown in Fig. 2 as total yield current versus photon energy. Note that the edge jump was only 14%. The corresponding $\chi(K)$ function[16] is shown in Fig. 3. The radial distribution function $|\Phi_2(r)|$, which was obtained by the Fourier transformation of $k^2\chi(k)$, is shown in Fig. 4. The subscript n of $\Phi_n(r)$ denotes the exponent of k employed in the Fourier transform, e.g., $k^n\chi(k)$. The nearest-neighbor and next-nearest-neighbor contributions to $\chi(k)$, $\chi_{NN}(k)$ and $\chi_{NNN}(k)$, shown in Figs. 5 and 6, were obtained by back-transforming nearest-neighbor and next-nearest-neighbor regions of $\Phi_0(r)$ using the window functions shown in Fig. 4.

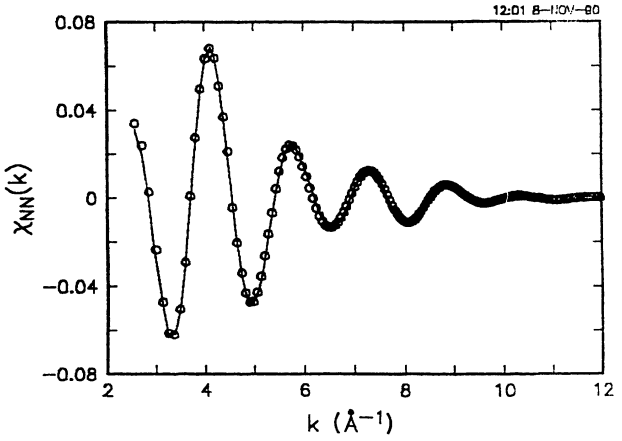

FIG. 5. Nearest-neighbor component of $\chi(k)$ for a Si:Ga sample (solid lines). Plotted symbols (○) are fitted model calculations $\chi_{calc}(k)$.

D. EXAFS analysis

The Ga K-edge EXAFS were analyzed only in terms of Ga-Si contributions, because the Ga concentration was only $x_{Ga}=1.8\times10^{-3}$. Ga-Ga nearest neighbors or next-nearest neighbors are expected to be very unlikely. Quantitative information on local structure around Ga atoms was obtained by fitting calculated model functions $\chi_{calc}(k)$ to the corresponding experimental functions $\chi_{NN}(k)$ and $\chi_{NNN}(k)$ over the range $k=3.8$–9.0 Å^{-1}. $\chi_{calc}(k)$ was calculated from the usual expression,[16]

$$\chi_{calc}(k)=\frac{N}{kr^2}\exp(-2k^2\sigma^2)F(k)\sin[2kr+\phi(k)] \ . \quad (2)$$

N is the number of neighbors, assumed to be Si as discussed above, at distance r from a Ga atom, with a Gaussian distance distribution of width σ. $F(k)$ is the backscattering amplitude for Si atoms which are nearest neighbors or next nearest neighbors of a Ga atom, as appropriate. $F(k)$ also includes inelastic scattering and other amplitude loss corrections. $\phi(k)$ is the total phase shift.

Since the primary goal of the EXAFS measurements on Si:Ga samples was to determine the Ga-to-Si nearest-neighbor distance, the backscattering amplitude including the damping function, $\exp(-2k^2\sigma^2)F(k)$, was calculated from the nearest-neighbor and next-nearest-neighbor amplitude functions taken from the $\chi(k)$ function being analyzed.[16]

The total phase shift $\phi(k)$ was determined from EXAFS measurements on crystalline GaP, with corrections[17] for changing the backscattering atom from P to Si. A second total-phase-shift function was determined from EXAFS measurements on the crystalline compound SiAs,[18] with corrections for changing the absorbing atom from As to Ga. These two phase-shift functions agree quite well with one another, as shown in Fig. 7. As discussed below, similar results were obtained with both of these phase shift functions. Also shown is the total-

TABLE II. Comparison of nearest-neighbor and next-nearest-neighbor distances from EXAFS measurements for Ga, Ge (Ref. 19), and As (Ref. 7) in silicon. Also shown are the strains $\epsilon=\Delta r/r$ with respect to near-neighbor distances in pure silicon. Values enclosed in parentheses are uncertain, as discussed in the text.

	r^{NN} (Å)	r^{NNN} (Å)	ϵ^{NN}	ϵ^{NNN}
Ga-Si	2.41±0.02	(3.91±0.06)	0.02	(0.02)
Ge-Si	2.37±0.02	3.85±0.06	0.01	0.00
As-Si	2.41±0.02	3.85±0.03	0.02	0.00
Si-Si	2.352	3.840	0	0

phase-shift function calculated from the theory-based tabulations of Teo and Lee.[17] E_0 values were shifted by 10 eV for GaP and by 30 eV for Teo-Lee calculated phase shifts plotted in Fig. 7.

In fitting $\chi_{calc}(k)$ and $\chi_{NN}(k)$ or $\chi_{NNN}(k)$, the only parameters being adjusted were the distance r^{NN} or r^{NNN} and the value of E_0, which enters the expression relating photon energy E and EXAFS wave vector k,

$$k=\left[\frac{2m}{\hbar^2}(E-E_0)\right]^{1/2} . \tag{3}$$

Standard deviations were calculated for the structural parameters, r^{NN} and r^{NNN}, determined by linearized least-squares fitting.[7] These error estimates correspond to the range of values which double the mean-square fitting error

$$\sum[\chi_{NN(NNN)}(k_i)-\chi_{calc}(k_i)]^2 . \tag{4}$$

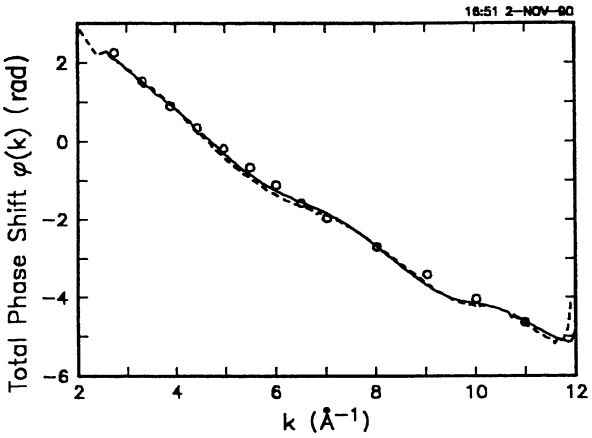

FIG. 7. Comparison of the total-phase-shift function $\phi(k)$ from EXAFS measurements on crystalline SiAs (solid line) and on crystalline GaP (dashed line), in each case corrected to apply for absorption by Ga and backscattering by Si using central atom and backscattering atom phase shifts from Teo and Lee (Ref. 17). E_0 [see Eq. (3)] for the GaP data was shifted by 10 eV from the absorption edge. Also shown (open circles) is the theory-based $\phi(k)$ from Teo and Lee (Ref. 17) with E_0 shifted by 30 eV.

E. EXAFS results

Best-fit comparisons with $\chi_{calc}(k)$ using SiAs derived phase shifts are shown in Figs. 5 and 6. Results were nearly identical for GaP-derived phase shifts. Values of r^{NN} and r^{NNN} obtained using SiAs- and GaP-derived phase shifts are 2.40 and 2.42 Å, averaging 2.41 A, with uncertainties estimated to be ±0.02 Å based on sensitivity and goodness of fit between $\chi_{calc}(k)$ and $\chi_{NN}(k)$. This value of $r^{NN}=2.41\pm0.02$ Å is 0.06 Å larger than the Si-to-Si nearest-neighbor distance in pure silicon, 2.35 Å.

The values of r^{NNN} are between 3.90 and 3.92 A, averaging 3.91 Å, with uncertainties estimated to be approximately 0.06 Å. This value of $r^{NNN}=3.91\pm0.06$ Å is 0.07 Å larger than the next-nearest-neighbor distance in pure silicon, 3.84 Å, and is quite surprising. In the other two similar systems which have been studied, Si:As (Refs. 6 and 7) and Si:Ge,[19,20] the nearest-neighbor As-to-Si and Ge-to-Si distances were larger than Si-Si by 0.06 and 0.03 Å, corresponding to local misfit strains $\epsilon^{NN}=\Delta r/r$ of 0.02 and 0.01, respectively, but the next-nearest-neighbor distances were the same, ±0.005 Å, as for Si-Si, or $\epsilon^{NNN}=0.00$ (see Table II). These results indicate that most of the atom size misfit for As or Ge in Si is taken up in the nearest-neighbor shell, with very little change in next-nearest-neighbor distances, as expected also from elasticity theory.[21]

A possible explanation for this unusual result of the EXAFS analysis for Ga-in-Si is that the next-nearest-neighbor distance obtained from EXAFS is in error because the Ga-to-Si next-nearest-neighbor distance distribution is asymmetrically broadened, by static and/or thermal disorder. As will be discussed later, $\chi_{NNN}(k)$ from the Si:Ga EXAFS measurements has a much smaller amplitude than the corresponding functions for Si:Ge and Si:As alloys, although $\chi_{NN}(k)$ functions have nearly the sample amplitudes for the three different materials (see Figs. 10 and 11). In each case, the backscattering is expected to be due almost entirely to Si, and in each case there are expected to be four nearest neighbors and 12 next-nearest neighbors. The lower amplitude of $\chi_{NNN}(k)$ for Si:Ga must then result from there being a wider spread of next-nearest-neighbor distances in this alloy. For broad distance distributions, fitting with Eq. (2) is expected to yield an accurate average distance r only if the broadening is Gaussian, or is at least symmetrical.[22] Low-temperature EXAFS measurements for Si:Ga would be valuable to determine whether or not the reduced amplitude of $\chi_{NNN}(k)$ and the surprisingly large value of

r^{NNN} are caused by thermal vibrations.

Another possible, but we believe less likely, explanation for the unusual result of the EXAFS analysis for Ga in Si is that the phase-shift functions obtained from GaP and from SiAs do not accurately reproduce the sum of central atom and backscattering phase shifts for the present Si:Ga alloys. If the linear component of the phase shift was in error by 0.06 Å, this would give r^{NN} and r^{NNN} both too large by 0.06 Å, and the correct values would then be $r^{NN}=2.35\pm0.02$ Å and $r^{NNN}=3.87\pm0.06$ Å, indicating that there is essentially no atom size misfit for Ga in Si. We believe that this is much less likely than the explanation given above based on asymmetrical broadening of the next-neighbor distance distribution causing error in the "average" distance determined from EXAFS. We know of no physical reason for the GaP and SiAs compounds to yield phase shifts which differ from the phase shift for Ga in Si when Teo-Lee[17]–type corrections have been appropriately included. The GaP- and SiAs-derived phase shifts apparently work well for evaluating nearest-neighbor and next-nearest-neighbor EXAFS for both As in Si (Ref. 7) and Ge in Si.[19]

III. DISCUSSION

A. Ga-to-Si nearest-neighbor distance and natural bond lengths

The Ga-to-Si nearest-neighbor distance determined for Si:Ga, 2.41±0.02 Å, is slightly larger than that for Ge to Si, 2.37±0.02 Å, and is the same as that for As to Si, 2.41±0.02 Å, as noted in Sec. II E and summarized in Table II. All of these nearest-neighbor distances were determined from EXAFS measurements on dilute alloys, with less than 10 at. % solute in silicon. To calculate β_{size}, the size-effect contribution per Ga atom to the average lattice strain, and to compare experimental r^{NN} values with values expected from theory-based tetrahedral covalent radii, the experimental r^{NN} values must be corrected for matrix effects, which cause nearest-neighbor distances in alloys to be composition dependent. For sp^3-bonded systems with diamond cubic or wurtzite structures, matrix effects have been discussed in terms of "natural" bond lengths and bond-bending and bond-stretching force constants.[23–25] For silicon, the natural bond length d^{nat}_{SiSi} is simply the nearest-neighbor distance in pure silicon. The Ga-to-Si natural bond length d^{nat}_{GaSi} is the nearest-neighbor distance which would occur for Ga in Si without constraints of the surrounding lattice. If d^{nat}_{GaSi} is larger than d^{nat}_{SiSi}, i.e., Ga is too large to fit onto an ideal lattice site of Si, the actual Ga-to-Si nearest-neighbor distance d_{GaSi} will fall somewhere between d^{nat}_{GaSi} and d^{nat}_{SiSi} and the misfit will be accommodated by having $d_{GaSi}<d^{nat}_{GaSi}$ and by having the matrix atoms somewhat displaced from ideal lattice sites.

For the dilute limit $x_{Ga}\approx0$, the relationship between the actual Ga-to-Si distance $d_{GaSi}(0)$ and the GaSi and SiSi natural bond lengths has been given by[23,26]

TABLE III. Natural bond lengths d_{nat} obtained from EXAFS measurements as discussed in the text, and calculated by summing tetrahedral covalent radii proposed by Pauling (Ref. 28), $d_{Pauling}$, and by Van Vechten and Phillips (Ref. 29), d_{VVP}.

	d_{nat} (Å)	$d_{Pauling}$ (Å)	d_{VVP} (Å)
Ga-Si	2.43±0.02	2.43	2.40
Ge-Si	2.39±0.02	2.39	2.40
As-Si	2.43±0.02	2.35	2.40

$$\frac{d_{GaSi}(0)-d^{nat}_{SiSi}}{d^{nat}_{GaSi}-d^{nat}_{SiSi}}=\epsilon\ . \tag{5}$$

Martins and Zunger[23] calculate ϵ from bond-stretching and bond-bending force constants α and β and obtain $\epsilon=0.58$ for silicon.[26] Shih *et al.*[24] obtain $\epsilon=0.75$ by neglecting both bond-bending force constants and movements of second shell neighbors.[27] Using the EXAFS result r^{NN} for $d_{GaSi}(0)$ and the actual Si-to-Si nearest-neighbor distance for d^{nat}_{SiSi} with Eq. (5) to calculate d^{nat}_{GaSi}, it makes only 0.01 Å difference whether $\epsilon=0.58$ or 0.75 is used. For consistency with earlier work,[7,9] we have used the later value, which yields the natural bond lengths for GaSi, GeSi, and AsSi given in Table III.

Natural bond lengths calculated using Pauling's tetrahedral covalent radii[28] for these elements (Si, 1.17 Å; Ga, 1.26 Å; Ge, 1.22 Å; and As, 1.18 Å) are also given in Table III and are in fair agreement with the EXAFS results except for As to Si, for which the Pauling estimate is 0.08 Å too small. Somewhat different covalent radii have been proposed by Van Vechten and Philips[29] (Si, 1.173 Å; Ga, Ge, and As, 1.225 Å) which give better agreement with the experimental results, as shown in Table III.

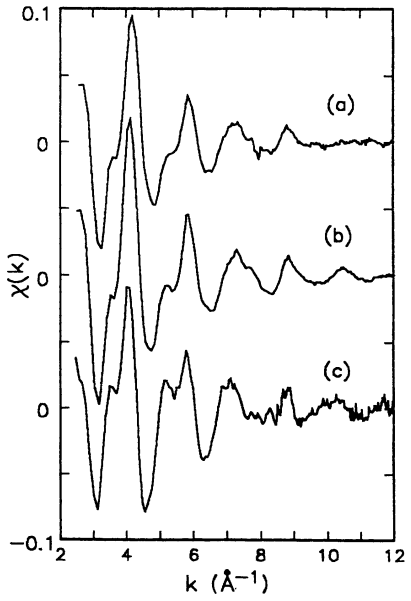

FIG. 8. EXAFS functions $\chi(k)$ for (a) Si:Ga, (b) Si:Ge (from Ref. 19), and (c) Si:As (from Ref. 7).

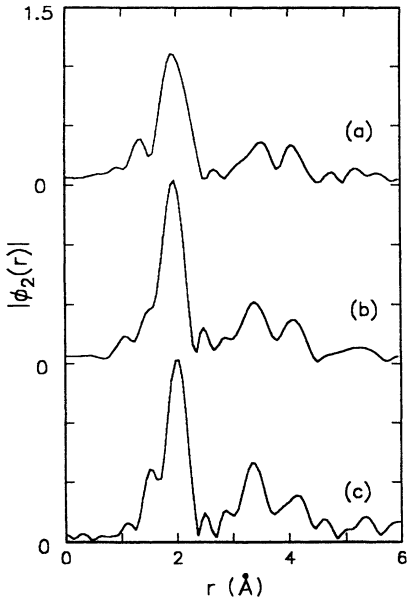

FIG. 9. EXAFS functions $|\Phi_2(r)|$ for (a) Si:Ga, (b) Si:Ge (from Ref. 19), and (c) Si:As (from Ref. 7).

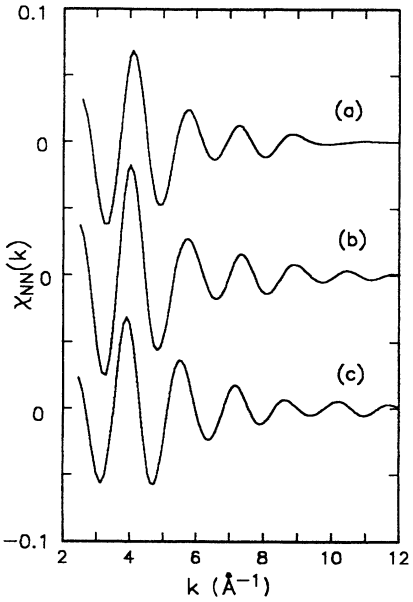

FIG. 11. Nearest-neighbor contributions $\chi_{NN}(k)$ for (a) Si:Ga, (b) Si:Ge (from Ref. 19), and (c) Si:As (from Ref. 7).

B. Comparisons of EXAFS for Si:Ga, Si:Ge, and Si:As

It is interesting to compare qualitatively the $\chi(k)$ functions for Si:Ga ($N_{Ga}=0.9\times10^{20}$cm^{-3}), Si:Ge ($N_{Ge}=50\times10^{20}$ cm^{-3})[19], and Si:As ($N_{As}=0.3\times10^{20}$ cm^{-3}) alloys,[7] which are shown in Fig. 8, and the $|\Phi_2(r)|$ functions for these alloys, shown in Fig. 9. The splittings of the first and second maxima of $\chi(k)$, at $k\approx4$ and 6 Å^{-1}, are present for each of the alloys to a varying degree. These splittings are caused by interferences between contributions from nearest, next-nearest, and third-nearest neighbors. Similar splittings are also seen in K-edge EXAFS for crystalline Si.[30] The nearest- and next-nearest-neighbor distances, obtained from EXAFS measurements, for these alloys are given in Table II.

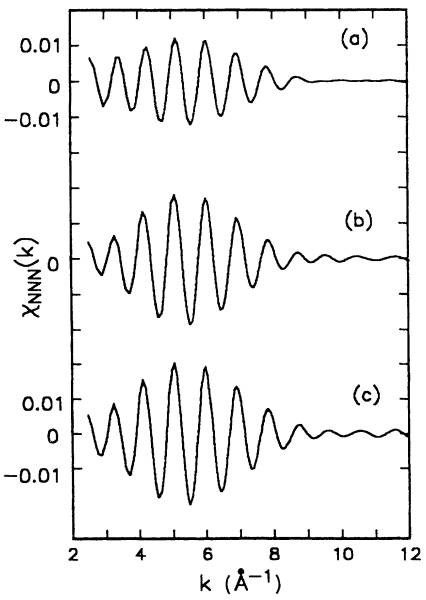

FIG. 10. Next-nearest-neighbor contributions $\chi_{NNN}(k)$ for (a) Si:Ga, (b) Si:Ge (from Ref. 19), and (c) Si:As (from Ref. 7).

An unusual aspect of the Si:Ga EXAFS data, already mentioned in Sec. II E, is the small amplitude of $\chi_{NNN}(k)$ compared with those of the Si:Ge and Si:As alloys, as shown in Fig. 10. $\chi_{NN}(k)$ have nearly the same amplitudes (see Fig. 11). In each case, the backscattering is expected to be due almost entirely to Si and in each case there are expected to be 12 next-nearest neighbors. The lower amplitude for Si:Ga may result from there being a wider spread of next-nearest distances in this alloy, because of additional static and/or thermal disorder affecting next-nearest neighbors in Si:Ga.

C. Lattice strain from holes

We assume, following Yokota,[31] that the net fractional change in the Si lattice constant per electrically active, substitutional Ga atom, β_{total}, originates from two independent components: (i) β_{size}, created by the local strain associated with different atomic radii, and (ii) β_h, resulting from the added holes affecting the lattice parameter.

The calculation of

$$\beta_{size}=\frac{a_{Si:Ga}^{size}-a_{Si}}{a_{Si}N_{Ga}} \tag{6}$$

requires the determination of the lattice parameter which Si:Ga would have because of local strain, since the natural Ga-Si bond length is larger than the natural Si-Si bond length, but without the doping effects of Ga. If the Ga-Si bond length was equal to the Si-Si bond length then

$a^{\text{size}}_{\text{Si:Ga}}$ would be unchanged from a_{Si}, and β_{size} would be zero. However, because

$$r_{\text{GaSi}} = r^{\text{NN}} > r_{\text{SiSi}} , \tag{7}$$

and therefore $d^{\text{nat}}_{\text{GaSi}} > d^{\text{nat}}_{\text{SiSi}}$, we obtain $a^{\text{size}}_{\text{Si:Ga}} > a_{\text{Si}}$ and $\beta_{\text{size}} > 0$.

Two different approaches to calculating $a^{\text{size}}_{\text{Si:Ga}}$ yield similar results. The first is the approach used in Ref. 5 for Si:As and based on Vegard's law. For the case of Si:Ga with Ga concentration $x_{\text{Ga}} = N_{\text{Ga}}/N_0$, where $N_0 = 5.00 \times 10^{22}$ cm^{-3} is the atomic density of pure Si, Vegard's law treats the lattice parameter as varying linearly with x_{Ga} between the lattice parameter of pure Si, a_{Si}, for $x_{\text{Ga}} = 0$, to the lattice parameter of a hypothetical zinc-blende-structure SiGa compound,

$$a_{\text{SiGa}} = (4/3^{1/2}) d^{\text{nat}}_{\text{GaSi}} , \tag{8}$$

for $x_{\text{Ga}} = 0.5$. Vegard's law predicts that

$$a^{\text{size}}_{\text{Si:Ga}}(x_{\text{Ga}}) = a_{\text{Si}} + 2x_{\text{Ga}}(a_{\text{SiGa}} - a_{\text{Si}}) , \tag{9}$$

and the resulting expression and numerical value for β_{size} are

$$\beta_{\text{size}} = \frac{2}{N_0}\left[\frac{d^{\text{nat}}_{\text{GaSi}} - d^{\text{nat}}_{\text{SiSi}}}{d^{\text{nat}}_{\text{SiSi}}}\right] = (1.4 \pm 0.3) \times 10^{-24} \text{ cm}^3 . \tag{10}$$

Another approach for calculating β_{size} is based on the fact that the lattice parameter a, which is measured by x-ray diffraction, for a random solution with an average lattice which has a diamond cubic structure, is related to the average nearest-neighbor bond length $\langle r \rangle = (\sqrt{3}/4)a$. For the dilute Si:Ga alloy of the present study, we assume that there are no Ga-Ga nearest neighbors, that the average Ga-Si bond length is given by r^{NN} from the EXAFS measurements, and that the average Si-Si bond length is given by the Si-Si natural bond length $d^{\text{nat}}_{\text{SiSi}}$. It follows that

$$\langle r \rangle = (2x_{\text{Ga}}) r^{\text{NN}} + (1 - 2x_{\text{Ga}}) d^{\text{nat}}_{\text{SiSi}} , \tag{11}$$

and this yields

$$\beta_{\text{size}} = \frac{2}{N_0}\left[\frac{r^{\text{NN}} - d^{\text{nat}}_{\text{SiSi}}}{d^{\text{nat}}_{\text{SiSi}}}\right] = (1.0 \pm 0.3) \times 10^{-24} \text{cm}^3 , \tag{12}$$

which is smaller than the result of Eq. (10). For further calculations, we take the average of these two values, of $\beta_{\text{size}} = (1.2 \pm 0.3) \times 10^{-24}$ cm^3. It is interesting to note that for Si:Ge, where both elements are isovalent and no doping occurs, β_{size} calculated from EXAFS measurements for Ge in Si in the same way as described here for Ga in Si agrees well with β_{total} obtained from lattice-parameter measurements on Si:Ge.[19]

The lattice strain created by holes in the valence band β_h can now be calculated,

$$\beta_h = \beta_{\text{total}} - \beta_{\text{size}} = (0.9 \pm 0.1) \times 10^{24} \text{ cm}^3 - (1.2 \pm 0.3) \times 10^{-24} \text{ cm}^3 = -(0.3 \pm 0.3) \times 10^{-24} \text{ cm}^3 . \tag{13}$$

Because of the small magnitude of β_h and the limited accuracy of our measurements of β_{total} and particularly of β_{size}, we can conclude only that β_h is between -0.6×10^{-24} cm^3 and zero.

D. Valence-band deformation potential

Deformation potentials were introduced originally by Bardeen and Shockley[32] to describe the effect of phonons on mobilities of electrons and holes in semiconductors. For the conduction band, the hydrostatic deformation potential is defined as

$$a_c = V\frac{dE_c}{dV} , \tag{14}$$

where E_c is the energy of the conduction-band edge. For the valence band, the corresponding hydrostatic deformation potential is defined as

$$a_v = V\frac{dE_v}{dV} , \tag{15}$$

where E_v is the energy of the valence-band edge. Keyes[33,34] has suggested that the same type of deformation potential is appropriate for describing the effects of electrons and holes from donors and acceptors on the lattice parameters of semiconductors. For donors, the relationship between the lattice parameter change due to electrons in the conduction band β_e and the conduction-band deformation potential a_c is given by

$$a_c = -3B\beta_e , \tag{16}$$

where B is the bulk modulus,[35] 0.61×10^{24} eV/cm^3 for Si. For acceptors, the relationship between the lattice parameter change due to holes in the valence band β_h and the valence-band deformation potential a_v is given by

$$a_v = +3B\beta_h . \tag{17}$$

Using the present results from measurements on the heavily doped Si:Ga samples, this corresponds to $a_v = -0.5 \pm 0.5$ eV for the valence-band hydrostatic deformation potential of silicon. Earlier, Cargill, Angilello, and Kavanagh[5] used similar measurements on heavily doped Si:As samples to obtain $\beta_e = -(1.8 \pm 0.4) \times 10^{-24}$ cm^3 and $a_c = +3.3 \pm 0.7$ eV for the conduction-band hydrostatic deformation potential of silicon.

Nolte, Walukiewicz, and Haller[36] reported hydrostatic deformation potentials derived from observed pressure derivatives of acceptor levels for Pt and Pd in Si. They obtained $a_v = +0.9$ eV, which is opposite in sign and somewhat larger in amplitude than the present experimental result.

First-principles calculations by Van de Walle and Martin[37] gave $a_v^{\text{theory}} = +1.3 \pm 1.0$ eV and $a_c^{\text{theory}} = +3.1 \pm 1.0$ eV. Recent *ab initio* calculations by Resta, Colombo, and Baroni[38] gave $a_v^{\text{theory}} = +1.5$ eV, in good agreement with

Ref. 37. In contrast with the earlier experimental measurements[5] for Si:As which agree well with the theoretically obtained deformation potential, the present experimental measurements for Si:Ga yield a value for the valence deformation potential which is smaller in magnitude and opposite in sign compared with the theoretical values. However, the theoretical and experimental values agree qualitatively, in the sense that the valence-band deformation potential is much smaller than the conduction-band deformation potential.

The pressure dependence of the optical band gap, $E_{\rm gap}=E_c-E_v$, is also related to the band-edge deformation potentials,

$$a_{\rm gap}=V\frac{dE_{\rm gap}}{dV}=a_c-a_v=-3B\beta_{eh}\ , \tag{18}$$

where $\beta_{eh}=\beta_e+\beta_h$. As reported by Welber *et al.*[39] from measurements of the pressure dependence of the Si band gap, $a_{\rm gap}=+1.7\pm0.1$ eV, which corresponds to $\beta_{eh}=-0.93\pm0.05\times10^{-24}$ cm^3. This agrees well with the earlier results of Laude, Pollak, and Cardona[40] and others,[41] but Balslev[42] reported values which were more than twice as large: $a_{\rm gap}=+3.8\pm0.5$ eV at 80 K and $a_{\rm gap}=+3.1\pm0.5$ eV at 295 K.

From EXAFS and x-ray diffraction measurements on Si:As (Ref. 5) and Si:Ga,

$$\begin{aligned}\beta_{eh}&=-(1.8\pm0.4)\times10^{-24}\ {\rm cm}^3\\&\quad+(-0.3\pm0.3)\times10^{-24}\ {\rm cm}^3\\&=-(2.1\pm0.5)\times10^{-24}\ {\rm cm}^3\end{aligned} \tag{19}$$

and

$$\begin{aligned}a_{\rm gap}&=(+3.3\pm0.7\ {\rm eV})-(-0.5\pm0.5\ {\rm eV})\\&=+3.8\pm0.9\ {\rm eV}\ ,\end{aligned} \tag{20}$$

which is substantially larger than values from pressure dependence of the optical band gap by most workers.[39–41]

Another method for determining $a_{\rm gap}$ is to measure the lattice parameter change caused by excitation of electron-hole pairs. In experiments reported by Gauster[43] *e-h* pairs were excited by pulses of MeV electrons, and the lattice-parameter change was determined by measuring the elastic strain, yielding $\beta_{eh}=-0.7\times10^{-24}$ cm^3, which corresponds to $a_{\rm gap}=+1.3$ eV. In more recent work by Buschert,[44] *e-h* pairs were created by optical excitation, and the lattice-parameter change was measured by x-ray diffraction, giving $\beta_{eh}=-5.0\times10^{-24}$ cm^3, and $a_{\rm gap}=9.1$ eV. These latter values of β_{eh} and $a_{\rm gap}$ are substantially larger than those determined from the pressure dependence of the optical band gap[39–42] and from the present doping experiments. Further work is needed to determine why the experimental values of $a_{\rm gap}$ and of β_{eh} from these *e-h*-pair generation experiments, from doping experiments, and from the pressure-dependent optical-band-gap experiments are so different.

It is interesting to note that most of the uncertainty in experimental values of β_h and a_v from the present doping experiments comes from uncertainty in $\beta_{\rm size}$, and in turn from uncertainty in the Ga-to-Si nearest-neighbor distance $r^{\rm NN}=2.41\pm0.02$ Å obtained from the EXAFS measurements. If $r^{\rm NN}=2.35$ Å instead of 2.41 Å, then $\beta_{\rm size}=0$, $\beta_h=\beta_{\rm size}=+0.9\times10^{-24}$ cm^3, and $a_v=+1.6$ eV. This would agree well with theoretical results[37,38] for a_v and with experimental results[39–41] for $a_{\rm gap}$. As discussed in Sec. II E, we believe the interpretation of the EXAFS measurements which gives $r^{\rm NN}=2.41$ Å to be correct, although there is some evidence which favors an interpretation which would indeed yield $r^{\rm NN}=2.35$ Å.

IV. CONCLUSIONS

Lattice expansion in heavily doped Si:Ga has been studied by EXAFS and double crystal x-ray diffraction. Two Si:Ga samples prepared by liquid-phase epitaxy (LPE) were studied. They had uniform Ga concentrations of 1.0×10^{20} and 1.5×10^{20} cm^{-3}, with comparable resistivities of 2.0×10^{-3} Ω cm. An average expansion per substitutional Ga atom of $+(0.9\pm0.1)\times10^{-24}$ cm^3 was observed. The average nearest-neighbor Si-Ga bond length was 2.41 ± 0.02 Å, which is 0.06 Å larger than the Si-Si nearest-neighbor distance in pure silicon. Combining these two results, the lattice strain per hole in the valence band is $-0.3\pm0.3\times10^{-24}$ cm^3, and the valence-band hydrostatic deformation potential is -0.5 ± 0.5 eV.

ACKNOWLEDGMENTS

We acknowledge M. Cardona (MPI, Stuttgart) for supplying the LPE material, R. F. Boehme for assistance with EXAFS, and J. Angilello, S. R. Herd, L. Hobbs, K. C. Pandey, J. Tersoff, A. Segmüller, and C. G. Van de Walle for useful discussions. One of us (K.K.) is grateful for partial support from IBM. This research was carried out in part at the National Synchrotron Light Source, Brookhaven National Laboratory, which is supported by the U. S. Department of Energy, Division of Materials Sciences and Division of Chemical Sciences (DOE Contract No. DE-AC02-76CH00016).

[1]B. C. Larson and J. F. Barhorst, J. Appl. Phys. **51**, 3181 (1980).
[2]P. Becker and M. Scheffler, Acta. Crystallogr. Sec. A **40**, C-341 (1984).
[3]M. Nemiroff and V. S. Speriosu, J. Appl. Phys. **58**, 3735 (1985).
[4]M. Servidori, Nucl. Instrum. Methods B **19/20**, 443 (1987).
[5]G. S. Cargill III, J. Angilello, and K. L. Kavanagh, Phys. Rev. Lett. **61**, 1748 (1988).
[6]A. Parisini, A. Bourret, A. Armigliato, M. Servidori, S. Solmi, R. Fabbri, J. R. Regnard, and J. L. Allain, J. Appl. Phys. **67**, 2320 (1990).
[7]A. Erbil, W. Weber, G. S. Cargill III, and R. F. Boehme, Phys. Rev. B **34**, 1392 (1986).
[8]B. Pajot and A. M. Stoneham, J. Phys. C **20**, 5241 (1987).
[9]Preliminary results were published earlier: K. L. Kavanagh, G. S. Cargill III, R. F. Boehme, and J. C. P. Chang, in *Ion Beam Processing of Advanced Electronic Materials,* edited by N. W. Cheung, A. D. Marwick, and J. B. Roberto, MRS Symposia Proceedings No. 147 (Materials Research Society,

Pittsburgh, 1989), p. 53. The present results, based on improved EXAFS measurements, are more precise than those reported earlier.

[10]W. H. Apple, Ph.D. thesis, University of Stuttgart, 1985 (unpublished).

[11]H. B. Harrison, Y. H. Li, G. A. Sai-Halasz, and S. Iyer, in *Materials Issues in Silicon Integrated Circuit Processing,* edited by M. Wittmer, J. Stimmell, and M. Strathman, MRS Symposia Proceedings No. 71 (Materials Research Society, Pittsburgh, 1986), p. 223. H. B. Harrison, S. S. Iyer, G. A. Sai-Halasz, and S. A. Cohen, Appl. Phys. Lett. **51**, 992 (1987).

[12]B. M. Arora, J. M. Castillo, M. B. Kurup, and R. P. Sharma, Radiat. Eff. **63**, 47 (1982).

[13]S. Bensoussan, C. Malgrange, and M. Sauvage-Simkin, J. Appl. Crystallogr. **20**, 222 (1987).

[14]J. Hornstra and W. J. Bartels, J. Cryst. Growth **44**, 513 (1978).

[15]A. Erbil, G. S. Cargill III, R. Frahm, and R. F. Boehme, Phys. Rev. B **37**, 2450 (1988).

[16]P. A. Lee, P. H. Citrin, P. Eisenberger, and B. M. Kincaid, Rev. Mod. Phys. **53**, 769 (1981).

[17]B. K. Teo and P. A. Lee, J. Am. Chem. Soc. **101**, 2815 (1979).

[18]T. Wadsten, Acta Chem. Scand. **19**, 1232 (1965); **23**, 331 (1969).

[19]M. Matsuura, J. M. Tonnerre, and G. S. Cargill III, Phys. Rev. B **44**, 3842 (1991).

[20]J. C. Woicik, C. E. Bouldin, M. I. Bell, J. O. Cross, D. J. Tweet, B. D. Swanson, T. M. Zhang, L. B. Soresen, C. A. King, J. L. Hoyt, P. Pianetta and J. F. Gibbons, Phys. Rev. B **43**, 2419 (1991).

[21]See, for example, J. D. Eshelby, in *Solid State Physics,* edited by F. Seitz and D. Turnbull (Academic, New York, 1956), Vol. 3, p. 79.

[22]P. Eisenberger and G. S. Brown, Solid State Commun. **29**, 481 (1979).

[23]J. L. Martins and A. Zunger, Phys. Rev. B **30**, 6217 (1984).

[24]C. K. Shih, W. E. Spicer, W. A. Harrison, and A. Sher, Phys. Rev. B **31**, 1139 (1985).

[25]M. F. Thorpe and E. J. Garboczi, Bull. Am. Phys. Soc. **35**, 781 (1990), and (unpublished).

[26]ϵ in Eq. (5), without superscripts, is used to keep the notation of Ref. 23. Its meaning is unrelated to those of the symbols ϵ^{NN} and ϵ^{NNN} used earlier in this paper.

[27]Martins and Zunger (Ref. 23) and Thorpe and Garboczi (Ref. 25) have argued that the approaches which ignore both bond-bending forces and movements of second-shell neighbors, like that of Shih *et al.* (Ref. 24), are fundamentally flawed and give approximately the right answer only because of cancellation of errors.

[28]L. Pauling, *The Nature of the Chemical Bond* (Cornell University Press, Ithaca, New York, 1960), p. 246.

[29]J. A. Van Vechten and J. C. Phillips, Phys. Rev. B **2**, 2160 (1970).

[30]J. C. Woicik and P. Pianetta, in *Synchrotron Radiation Research: Advances in Surface Science,* edited by R. Z. Bachrach (Plenum, New York, 1990).

[31]I. Yokota, J. Phys. Soc. Jpn. **19**, 1487 (1964).

[32]J. Bardeen and W. Shockley, Phys. Rev. **80**, 72 (1950).

[33]R. W. Keyes, IBM J. Res. Dev. **5**, 266 (1961).

[34]R. W. Keyes, in *Solid State Physics,* edited by H. Ehrenreich, F. Seitz, and D. Turnbull (Academic, New York, 1967), Vol. 20, p. 37.

[35]W. Kress, in *Numerical Data and Functional Relationships in Science and Technology,* edited by K. H. Hellwege, Landolt-Börnstein, New Series, Vol. 17a (Springer, Berlin, 1982), p. 64.

[36]D. D. Nolte, W. Walukiewicz, and E. E. Haller, Phys. Rev. B **36**, 9392 (1987).

[37]C. G. Van de Walle and R. M. Martin, Phys. Rev. Lett. **62**, 2028 (1989). See also, C. G. Van de Walle and R. M. Martin, Phys. Rev. B **39**, 1871 (1989).

[38]R. Resta, L. Colombo, and S. Baroni, Phys. Rev. B **41**, 12358 (1990).

[39]B. Welber, C. K. Kim, M. Cardona, and S. Rodriguez, Solid State Commun. **17**, 1021 (1975).

[40]L. Laude, F. H. Pollak, and M. Cardona, Phys. Rev. B **3**, 2623 (1971).

[41]See Ref. 40, and papers cited therein.

[42]I. Balslev, Phys. Rev. **143**, 636 (1966).

[43]W. B. Gauster, Phys. Rev. **187**, 1035 (1969).

[44]J. R. Buschert, Ph.D. thesis, Purdue University, 1989 (unpublished); J. R. Buschert and R. Colella, Solid State Commun. **80**, 419 (1991).